J Neurophysiol 103: 3070–3083, 2010.
First published March 24, 2010; doi:10.1152/jn.00913.2009.

Computational Analysis of the Impact of Chronic Stress on Intrinsic and Synaptic Excitability in the Hippocampus

Rishikesh Narayanan and Sumantra Chattarji
National Centre for Biological Sciences, Bangalore 560065, India

Submitted 19 October 2009; accepted in final form 15 March 2010

Narayanan R, Chattarji S. Computational analysis of the impact of chronic stress on intrinsic and synaptic excitability in the hippocampus. *J Neurophysiol* 103: 3070–3083, 2010. First published March 24, 2010; doi:10.1152/jn.00913.2009. Dendritic atrophy and impaired long-term synaptic potentiation (LTP) are hallmarks of chronic stress-induced plasticity in the hippocampus. It has been hypothesized that these disparate structural and physiological correlates of stress lead to hippocampal dysfunction by reducing postsynaptic dendritic surface, thereby adversely affecting the availability of synaptic inputs and suppressing LTP. Here we examine the validity of this framework using biophysical models of hippocampal CA3 pyramidal neurons. To statistically match with the experimentally observed region specificity of stress-induced atrophy, we use an algorithm to systematically prune three-dimensional reconstructions of CA3 pyramidal neurons. Using this algorithm, we build a biophysically realistic computational model to analyze the effects of stress on intrinsic and synaptic excitability. We find that stress-induced atrophy of CA3 dendrites leads to an increase in input resistance, which depends exponentially on the percentage of neuronal atrophy. This increase translates directly into higher spiking frequencies in response to both somatic current injections and synaptic inputs at various locations along the dendritic arbor. Remarkably, we also find that the dendritic regions that manifest atrophy-induced synaptic hyperexcitability are governed by the region specificity of the underlying dendritic atrophy. Coupled with experimentally observed modulation of *N*-methyl-D-aspartate receptor currents, such hyperexcitability could tilt the balance of plasticity mechanisms in favor of synaptic potentiation over depression. Thus paradoxically, our results suggest that stress may impair hippocampal learning and memory, not by directly inhibiting LTP, but because of stress-induced facilitation of intrinsic and synaptic excitability and the consequent imbalance in bidirectional synaptic plasticity.

INTRODUCTION

Severe and prolonged stress leads to deficits in hippocampal function at multiple levels of neural organization (McEwen 1999). Investigations into cellular mechanisms underlying stress-induced impairments have focused primarily on two common metrics of hippocampal plasticity: one structural and the other electrophysiological. First, animal models of chronic stress cause dendritic atrophy in hippocampal CA3 pyramidal neurons (Magarinos and McEwen 1995b). This dendritic atrophy, in turn, has been hypothesized to underlie hippocampal volume loss reported in clinical studies of chronic stress-related disorders in humans (Sapolsky 2001, 2002). Second, rodent models of stress also disrupt synaptic plasticity mechanisms such as long-term potentiation (LTP) and depression (LTD) that play important roles in hippocampal learning and memory (Kim and Diamond 2002). A potential convergence between these two lines of enquiry is provided by the *N*-methyl-D-aspartate type of glutamate receptor (NMDAR), which is involved in the induction of LTP (Collingridge et al. 1983) and LTD (Debanne et al. 1998), as well as stress-induced dendritic atrophy in CA3 pyramidal cells (Magarinos and McEwen 1995b).

Although specific effects of stress on hippocampal neuronal structure and synaptic physiology have been identified experimentally, we still lack a mechanistic and quantitative understanding of how these disparate morphological and physiological changes interact to affect hippocampal output at the cellular and network levels. This gap is especially striking because changes in dendritic architecture can affect intrinsic excitability of neurons in ways that do not necessarily have to be mediated directly through modulation of synaptic transmission (Mainen and Sejnowski 1996; Sjostrom et al. 2008) and because there is experimental data suggesting a link between stress and hippocampal hyperexcitability (Conrad et al. 2004; Kole et al. 2004; Pavlides et al. 2002).

Is there a conceptual framework for unifying these findings? Specifically, can the morphological and electrophysiological correlates of stress interact or influence each other? If so, can such interactions explain stress-induced deficits in LTP? An intuitive way of thinking about these data are embodied in the view that stress-induced loss of postsynaptic dendritic surface adversely affects the availability of synaptic inputs, thereby reducing the neuron's ability to support normal LTP. Another view is rooted in a theoretical framework that has been widely used to interpret experimental findings on hippocampal LTP/LTD—the Bienenstock-Cooper-Munro (BCM) rule (Abraham and Bear 1996; Bienenstock et al. 1982). According to the BCM rule, the threshold for induction of LTP is itself modifiable and is dependent on the average postsynaptic activity. Stress has been proposed to induce a rightward shift in the BCM-like plasticity profile, thereby setting the threshold for LTP induction so high as to lower the probability of eliciting LTP after chronic stress (Kim and Diamond 2002; Kim and Yoon 1998). Although much of the existing electrophysiological data on stress-induced modulation of synaptic plasticity is broadly consistent with the abstract framework offered by the BCM theory, it does not provide any mechanistic explanation as to how the specific morphological or physiological effects of stress may lead to a shift in the plasticity profile (Diamond et al. 2004). To reconcile this broad spectrum of observations and ideas, and to bridge the gap between them, we developed a computational framework to analyze the effects of chronic stress-induced plasticity on synaptic and neuronal excitability of hippocampal CA3 pyramidal cells.

Address for reprint requests and other correspondence: S. Chattarji, National Ctr. for Biological Sciences (NCBS), GKVK Campus, Bangalore 560065, India (E-mail: shona@ncbs.res.in).

METHODS

At the single cell level, we divided the problem of analyzing the effects of dendritic atrophy on CA3 pyramidal cell electrophysiology into two parts: *1*) subjecting a normal CA3 pyramidal cell dendritic tree to atrophy according to data from experiments (we refer to the process of subjecting model neurons to atrophy as pruning) and *2*) imposing active and passive properties of actual CA3 cells on these model cells (normal and atrophied) and analyzing the functional changes.

To solve the first of these two parts, we developed an algorithm that induces systematic, region-specific remodeling of dendritic morphology as per experimental data on atrophy (Narayanan et al. 2005). We used digital reconstructions of CA3b pyramidal neurons from the Duke-Southampton Archive (DSArchive; Cannon et al. 1998) as inputs to the algorithm (control CA3b pyramidal cells). Experimental data from the study of Vyas et al. (2002) provided statistical data on dendritic lengths and branching points along various segments of the dendritic tree for both control and stressed animals. Using these, we have previously shown (Narayanan et al. 2005) that our algorithm is capable of *1*) replicating experimental segment-wise atrophy in model three-dimensional neuronal reconstructions; *2*) pruning these three-dimensional reconstructions to various levels, with region-specificity maintained through the pruning process. The use of our algorithm to induce region-specific dendritic atrophy for analyzing the effects of remodeling has a number of advantages (also see Narayanan et al. 2005):

1) It improves on previous studies that have established correlations between structure and function of groups of neurons (Krichmar et al. 2002; Mainen and Sejnowski 1996; van Ooyen et al. 2002; Vetter et al. 2001); our algorithm allows us to induce specific structural changes in a given neuron and examine its functional consequences in the same neuron, thereby enabling us to establish a causal link between stress-induced remodeling and its biophysical effects.

2) The use of multiple neurons to arrive at the relationship between structure and function of neurons has the potential pitfall that biologically observed statistical variability across neurons might cause a nonatrophied neuron (from a control animal) to elicit functional responses similar to an atrophied neuron (from a stressed animal). Our algorithm uses a single neuron to causally construct the structure–function relationship.

3) The algorithm provides us with trees with varying percentages of atrophy, in a region-specific manner, of the original dendritic tree. This enables us to analyze the functional form of the relation of various biophysical parameters to dendritic length (as in Fig. 1, *B* and *C*, for instance), rather than just having two instances (one corresponding to "Control" and other corresponding to "Stress").

4) It helps in analyzing the effects of basal-alone and apical-alone pruning while maintaining "tree-consistency" all along. That is, trees at a given atrophy level are subtrees of all trees with lower levels of atrophy, irrespective of whether basal tree or apical tree alone is pruned (the trees that are used in arriving at Fig. 2*F*, for instance).

5) Comparison of the outcomes of synaptic stimulation to the same dendritic point in two different trees (the dendritic points in Fig. 2*A*, for instance) is made possible as the atrophied tree is a subtree of the control tree. This, along with maintenance of tree consistency, makes sure that there are no spurious effects of branching patterns on the propagation of information along the dendritic tree (Vetter et al. 2001).

6) It provides an opportunity to address questions on region-specific changes in various biophysical readouts as a result of region-specific atrophy (as brought out in Fig. 2).

At the end of the pruning process, we would thus have "control" neuronal reconstructions along with their "stress" counterparts with varying percentages of atrophy, in a region-specific manner, of the original dendritic length. We used these reconstructions for studying the functional implications of region-specific remodeling in the fol-

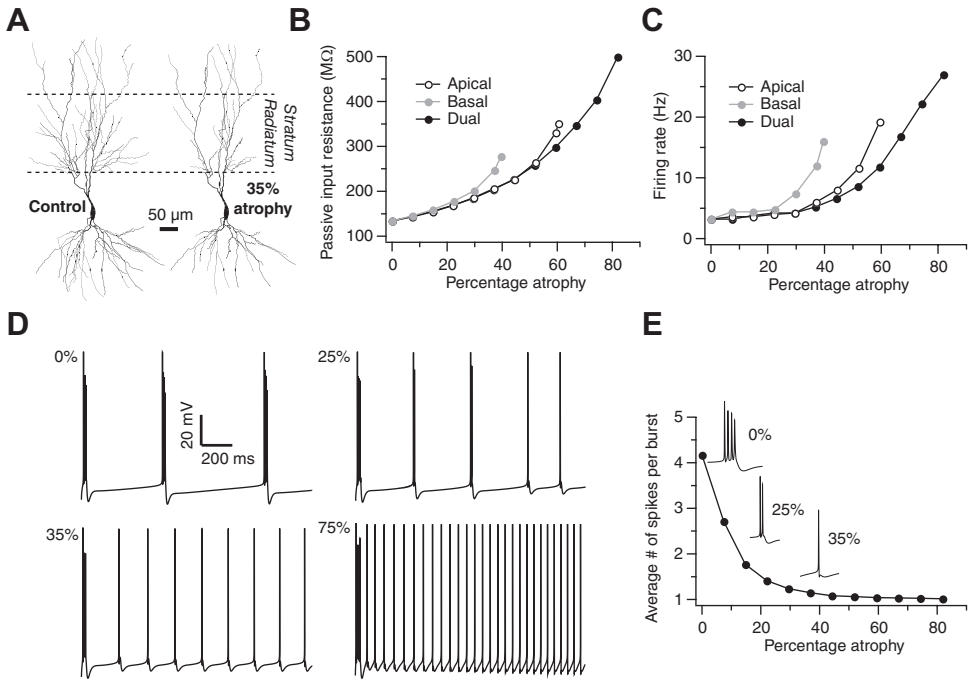

FIG. 1. Atrophy alters electrophysiological properties of CA3 pyramidal cells. *A*: example of dendritic atrophy (35% atrophy, *right*), induced by the pruning algorithm, in which a typical Control (*left*) neuron from the Duke Southampton archive is subjected to 35% reduction in dendritic length (13,669 to 8,642 μm) and 23% reduction in number of branch points (63 to 48). In conformity with experimental results, maximal atrophy may be observed in the stratum radiatum region (delineated by dotted lines; 100–350 μm from the soma) and in the mid-basal regions. *B*: passive input resistance as a function of the percentage of atrophy (percentage atrophy is calculated, in all cases, with respect to the total dendritic length of the Control neuron) of either apical (black open circles) or basal (gray) dendrites alone or both together (black closed circles). *C*: action potential firing rates of CA3 pyramidal cells as a function of percentage of atrophy. Notations as in *B*. *D*: a transition in action potential firing patterns, from burst firing to regular spiking, exhibited by a control neuron (0% pruning) and neurons with varying degrees of pruning (35, 45, 75%). *E*: average number of spikes per burst, computed over a period of 5 s of current injection, as a function of percentage of atrophy. *Insets* depict single bursts, which are magnified versions of corresponding plots in *D*, generated by neurons that underwent 35 or 45% or no atrophy (0%).

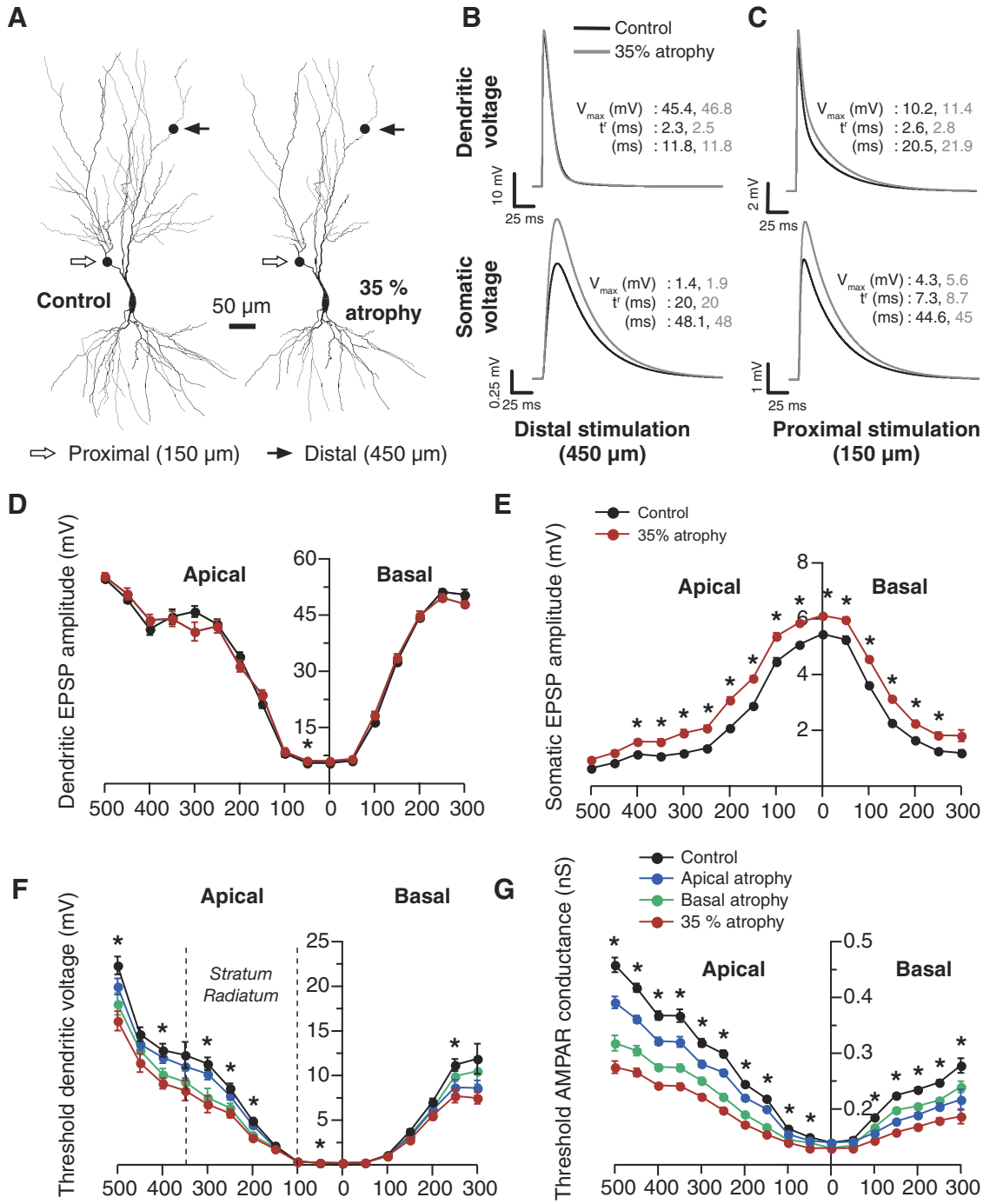

FIG. 2. Region-specific atrophy induces region-specific increase in synaptic excitability in a passive dendritic tree. *A*: reconstructions showing a Control neuron and the same neuron after 35% atrophy imposed by the pruning algorithm. Synaptic locations of distal and proximal stimulation sites, used in *B* and *C*, are indicated. As the dendritic tree with 35% atrophy is obtained from the Control tree, it may be considered as a subtree with both distal and proximal locations corresponding to the same dendritic compartments as in its Control counterpart. *B*: excitatory postsynaptic potentials (EPSP) evoked by the injection of a single AMPA-excitatory postsynaptic current (EPSC), at a distal location (450 μm from the soma) on a passive dendrite, as measured at the site of injection (*top*, Dendritic Voltage) or the soma (*bottom*, Somatic Voltage). *C*: similar to *B*, with synaptic stimulation delivered at a more proximal dendritic site (150 μm from the soma). For *B* and *C*, V_{max} corresponds to the maximum value of voltage attained, t^r is the time taken to rise from 0 mV to V_{max}, and τ is the decay time-constant obtained by fitting an exponential to the decay phase of the trace. *D*: local dendritic response amplitude to synaptic stimulation [with a 4 nS AMPA receptor (AMPAR) conductance] of various dendritic compartments as a function of radial distance of that compartment from the soma. *E*: somatic response amplitude to synaptic stimulation (with a 4 nS AMPAR conductance) of various dendritic compartments as a function of radial distance of that dendritic compartment from the soma. A significant increase in excitability across all regions is evident in the atrophied tree compared with the control tree. In *D* and *E*, black shows mean and SE for Control neuron, and red shows mean and SE for neuron with 35% atrophy. *F*: minimum local dendritic voltage required to elicit a 0.2 mV somatic response with synaptic stimulation of various dendritic compartments plotted as a function of radial distance of the dendritic compartment from the soma. *G*: minimum local dendritic AMPAR conductance required to elicit a 0.2 mV somatic response with synaptic stimulation of various dendritic compartments plotted as a function of radial distance of the dendritic compartment from the soma. In *F* and *G*, black shows mean and SE for Control neuron, red shows mean and SE for neuron with 35% atrophy, blue shows mean and SE for neuron with basal-alone pruning, and green shows mean and SE for neuron with apical-alone pruning. In *D–F*, $*P < 0.001$, Student's *t*-test, Control vs. 35% atrophy.

lowing sections. In doing this, we assumed that ion channel densities in CA3 pyramidal cells do not change with stress, because of lack of experimental data.

CA3 pyramidal cell model

We imposed passive and active membrane properties on three-dimensional reconstructions as in the modeling study by Migliore et al. (1995). The membrane resistivity r_m was set at 60 kΩ cm^2, axial resistivity r_a was 200 Ωcm, and membrane capacitance c_m was 0.75 μF/cm^2 throughout all compartments. The model included a single Na^+ channel, three types of voltage-gated calcium channels (VGCCs)—Ca_N, Ca_L, and Ca_T—three Ca^{2+}-independent K^+ channels (K_{DR}, K_M, and K_A), and two Ca^{2+}-dependent K^+ channels (K_C and K_{AHP}). Kinetics and distributions of all the channel conductances were adapted from Migliore et al. (1995), with the following exceptions: *1*) Na^+ and K_{DR} channels were distributed throughout the neuron (Magee and Johnston 1995) rather than being concentrated only at the soma and perisomatic compartments and *2*) kinetics and distribution for the K_A channel were adapted from Migliore et al. (1999). Different kinetic schemes are used for proximal and distal regions (with respect to distance from soma) of the dendrites and maximal conductance increases linearly with distance from soma.

These exceptions were made to incorporate the current understanding of channel distributions across pyramidal neurons. Additionally, internal and external calcium concentration dynamics were controlled using buffering, pumping, and radial diffusion mechanisms distributed uniformly over the entire neuron (Migliore et al. 1995). The neuronal model does not have an explicit axonal compartment (Migliore et al. 1995).

The CA3 region contains two classes of pyramidal cells: *1*) intrinsically bursting and *2*) regular spiking (Hablitz and Johnston 1981; Migliore et al. 1995; Wong and Prince 1978). An intrinsically bursting CA3 neuron responds to a brief pulse of somatic current injection with a series of action potentials placed close together in time, with reducing amplitudes, followed by a longer period of afterhyperpolarization. A regular spiking cell, on the other hand, responds with a single spike at regular intervals. These two cell types also repeat such bursting and regular-spiking behaviors with longer lasting current injections (Migliore et al. 1995). The bursting cells, further, display contrasting firing patterns depending on the magnitudes of current injections. With lower current injections they tend to burst, whereas with higher current injections they spike regularly (Migliore et al. 1995). Hence, we first replicated the electrophysiological properties of intrinsically bursting CA3 pyramidal cells with somatic current injections (Fig. 1*D*; 0% pruning). We achieved this by setting ion channel parameters in the model cell without any atrophy (i.e., control neuron) to satisfy the following criteria established by previous studies (Migliore et al. 1995): *1*) a brief stimulation (1.5 nA, 3 ms) elicits a burst with approximately four spikes with progressively reducing amplitudes; *2*) the cell exhibits continuous bursting with persistent current injection of 0.15 nA; and *3*) the cell displays continuous firing in the regular spiking mode with persistent stimulation at 0.6 nA (Migliore et al. 1995). The default values of parameters for a typical bursting neuron were as follows: reversal potentials for various ions (in mV), $V_{Na} = 50$ and $V_K = -91$; maximal conductance for the ion channels, in S/cm^2, $\hat{g}_{Na} = 0.018$, $\hat{g}_{KDR} = 0.0088$, $\hat{g}_{CaL} = 0.0025$, $\hat{g}_{CaN} = 0.0028$, $\hat{g}_{CaT} = 0.00025$, $\hat{g}_{KC} = 0.0008$, $\hat{g}_{KM} = 0.00001$, $\hat{g}_{KAHP} = 0.0003$; maximal conductance for the A-type K-channel $\hat{g}_{KA}$ is set at 0.007 S/cm^2 at the soma and linearly increases with a slope 0.011 s/cm^2 for every 100 μm of distance along the dendrites. An intrinsically spiking cell was tuned to regularly spike at all current injection levels and was modeled by increasing the calcium independent potassium channel conductance (K_{DR} and K_A) (Migliore et al. 1995). The changes in conductances to obtain an intrinsically spiking cell are (in S/cm^2) $\hat{g}_{KDR} = 0.03$, $\hat{g}_{Na} = 0.025$, and $\hat{g}_{KM} = 0.0001$.

Synaptic inputs

Simulations used NMDAR and AMPA receptor (AMPAR) currents to synaptically stimulate the dendrites. Both receptors were modeled using two-state Markovian kinetics (Destexhe et al. 1998). Magnesium block of NMDA receptors was incorporated by a voltage-dependent modulation of NMDA conductance (Jahr and Stevens 1990) with an extracellular magnesium concentration set at 2 mM.

Default parameters for the synapses in simulations are as follows: reversal potentials, $E_{NMDA} = E_{AMPA} = 0$ mV; rising time, $t^r_{NMDA} = 5$ ms and $t^r_{AMPA} = 2$ ms; decaytime constant, $\tau_{NMDA} = 55$ ms and $\tau_{AMPA} = 5$ ms (Kole et al. 2002; Traub et al. 1996).

NMDAR and AMPAR current measurements

After initializing colocalized AMPAR-NMDAR synapses, stimulation induced excitatory postsynaptic currents (EPSCs) were measured under "voltage-clamp" conditions. AMPAR-EPSCs were obtained at a holding potential of −65 mV and by setting the maximal NMDAR conductance, $\hat{g}_{NMDA} = 0$ S, whereas NMDAR currents were obtained at a holding potential of +60 mV (to relieve the voltage-dependent magnesium block) and by setting the maximal AMPAR conductance, $\hat{g}_{AMPA} = 0$ S (Kole et al. 2002). Figure 3*D* depicts typical AMPAR and NMDAR EPSCs. In obtaining these traces, the total AMPAR conductance was set at a constant 10 nS and the total NMDAR conductance was calculated according to the experimentally reported increase in the NMDA-EPSC/AMPA-EPSC ratio (control: 0.26; stress: 0.44), as AMPAR-EPSCs are not affected by stress (Kole et al. 2002). These conductances were equally distributed across all the compartments in the stratum radiatum, with each compartment getting its share based on its surface area relative to the total area of compartments within stratum radiatum.

Simulation implementation

A Linux system running on a Pentium IV processor was used for all computations. The dendritic remodeling algorithm (Narayanan et al. 2005) was implemented using C++. The java-based CVAPP tool kit (which is available along with the DSArchive; Cannon et al. 1998) was used to convert three-dimensional morphology in SWC files (obtained either from the DSArchive or as outputs of the pruning algorithm; Narayanan et al. 2005) to NEURON-compatible HOC files. Compartments were subdivided into smaller segments not longer than 10% of the length constant λ at 100 Hz. All neuronal simulations were performed using the NEURON simulation environment (Hines and Carnevale 1997) in conjunction with NMODL (Hines and Carnevale 2000). Integration time constant was set at 25 μs for all NEURON simulations. All simulations were run at 37°C with temperature dependencies taken care according to individual channel kinetics.

Computational details

We computed the firing rate of a neuron by dividing the number of spikes in a time interval by the size of the interval. In all cases, spikes are counted if they cross the 0 mV threshold. Passive input resistance of a neuron is computed with a depolarizing somatic current step (Migliore et al. 1995). The ratio of the steady-state somatic voltage to this depolarizing current then gives the passive input resistance.

RESULTS

Strategy

Our analysis of the functional consequences of stress-induced plasticity has two important components based on earlier studies: *1*) a previously characterized and biologically realistic model of hippocampal CA3 pyramidal neurons that captures

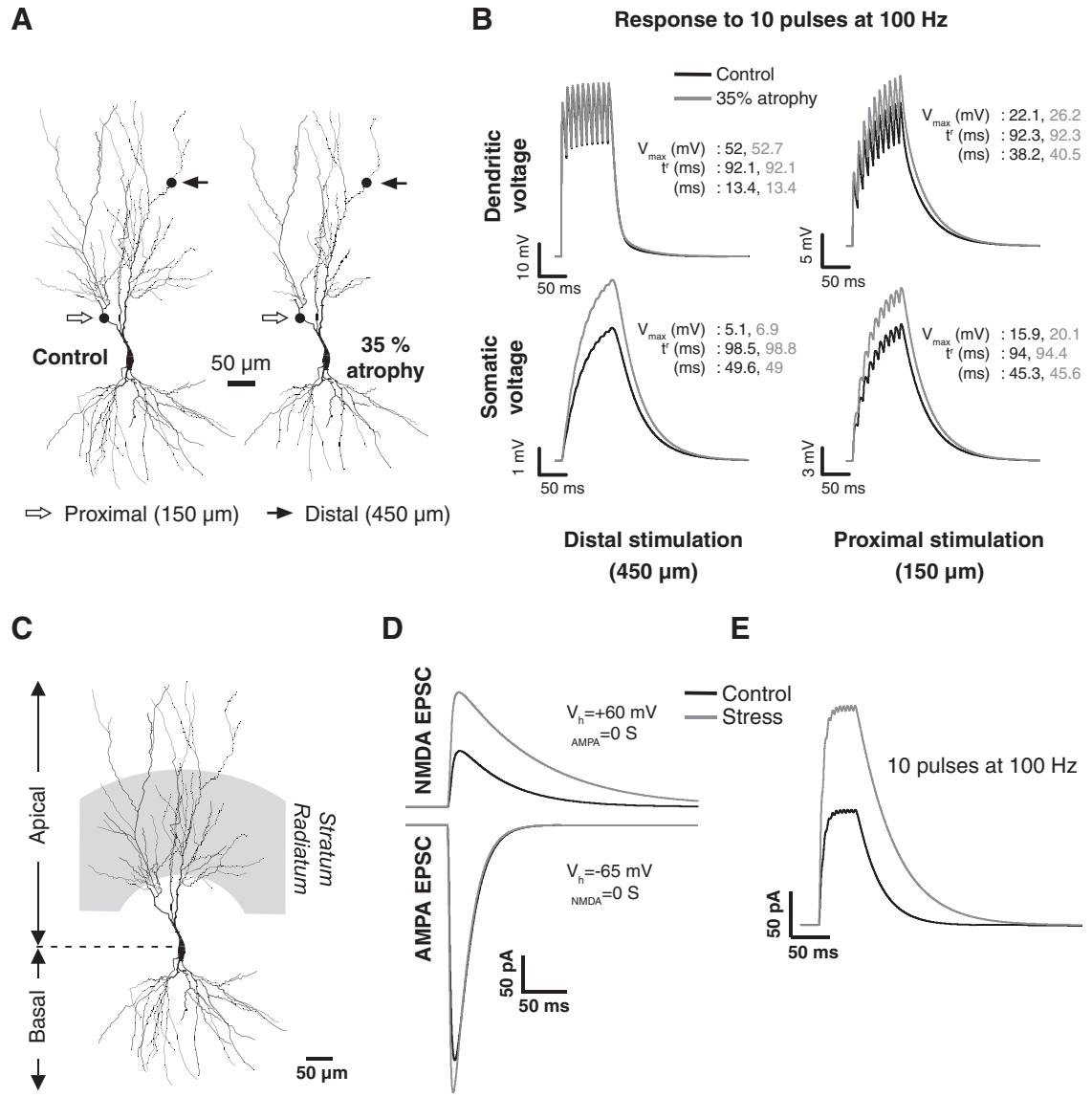

FIG. 3. *A*: reconstructions showing a Control neuron and the same neuron after 35% atrophy imposed by the pruning algorithm. Synaptic locations of distal and proximal stimulation sites, used in *B* and *C*, are indicated. As the dendritic tree with 35% atrophy is obtained from the Control tree, it may be considered as a subtree with both distal and proximal locations corresponding to the same dendritic compartments as in its Control counterpart. *B*: EPSPs recorded at the same dendritic (*top*) and somatic (*bottom*) sites in response to 10 EPSCs delivered at the distal dendritic point at a frequency of 100 Hz, with stimulation site located at 450 (*left*) and 150 μm (*right*) from the soma. V_{max} corresponds to the maximum value of voltage attained, t^r is the time taken to rise from 0 mV to V_{max}, and τ is the decay time-constant obtained by fitting an exponential to the decay phase of the trace. *C*: representative neuron depicting the region of stimulation (shaded region; stratum radiatum) for eliciting synaptic responses in *D* and *E*. *D*: somatic current traces recorded, at depolarizing (+60 mV) and hyperpolarizing (−65 mV) holding potentials, from Control (black) and Stress (gray) pyramidal cells. Responses are obtained by stimulating synapses located all over stratum radiatum. *Top*: *N*-methyl-D-aspartate receptor (NMDAR)-mediated EPSCs ($V_h = +60$ mV; $g_{AMPA} = 0$ S). *Bottom*: AMPAR-mediated EPSCs ($V_h = -65$ mV; $g_{NMDA} = 0$ S). *E*: NMDAR-EPSCs, recorded at +60 mV, in response to a stimulus train of 10 pulses at 100 Hz. Note the increase in NMDAR-EPSC summation found in the Stress cell compared with Control cells.

many of its key biophysical and electrophysiological properties (see METHODS) and *2*) experimental data from single-neuron morphometric and electrophysiological analyses of the changes in dendritic structure and synaptic function caused by chronic stress in CA3 pyramidal cells. In other words, the basic model of a "control" or "unstressed" neuron, as well as the modulation of its structure and function by stress, is guided by previously reported experimental data obtained from CA3 pyramidal neurons in rats; the specific features of the data related to these cellular effects will be described as they are incorporated into our model in later sections. The important step in our analysis involves a merger of the above two elements with the aim of establishing a causal link between stress-induced changes in single-neuron properties and their functional consequences. The conventional experimental approach to identifying the cellular correlates of behavioral stress has been to compare two different populations of neurons, derived from separate groups of stressed and unstressed animals. In contrast, the computational strategy presented here allows us to compare a range of biophysical and electrophysiological parameters before and after the application of stress-induced changes in the same model neuron, thereby enabling us to quantify the direct consequences of a specific stress-related parametric change within the same neuron.

Region-specific dendritic atrophy in three-dimensional neuronal reconstructions

We first focus on the most extensively studied morphological effect of chronic stress at the single-cell level. Dendritic atrophy in CA3 pyramidal neurons, caused by many rodent models of chronic or repeated stress, is manifested as a reduction in total dendritic length (~30%), as well as a decrease in total number of branch points (~30%) (Magarinos and McEwen 1995b; Vyas et al. 2002). Importantly, detailed morphometric analysis indicates that such atrophy is confined to specific dendritic regions of the CA3 pyramidal cell. In other words, the magnitude of the atrophy varies as a function of the radial distance of the affected dendritic segment from the soma. Specifically, the most pronounced atrophy in CA3 pyramidal cells is restricted largely to the stratum radiatum region of apical dendrites, with other regions undergoing little or no atrophy (Kole et al. 2004; Magarinos and McEwen 1995a; Magarinos et al. 1996; Vyas et al. 2002).

What are the functional consequences of such dendritic region-specific (throughout this article we refer to region-specific to denote dendritic regions and not hippocampal subregions—CA1, CA3, etc.) structural changes? To address this question, we make use of a computational algorithm that uses statistics from morphometric analyses to remodel neuronal reconstructions (Narayanan et al. 2005). This algorithm, through an iterative process, systematically imposes atrophy in three-dimensional neuronal reconstructions while maintaining region specificity, as well as the experimentally observed proportion of atrophy in dendritic length and branch points (for the rest of the paper, we use the generic term "dendritic atrophy" to denote both reduction in dendritic length and debranching). A rigorous analysis of this dendritic pruning algorithm, which replicates key features of experimental data on stress-induced dendritic atrophy in area CA3, has been presented earlier (Narayanan et al. 2005). Briefly, as our starting point for this analysis, we take a three-dimensionally reconstructed CA3 pyramidal neuron (Fig. 1*A*) from the Duke/Southampton archive and elicit dendritic atrophy in this neuron by subjecting it to our pruning algorithm; the outcome of this dendritic atrophy is depicted in Fig. 1*A*. As depicted in Fig. 1 and Supplemental Fig. S1,[1] the stratum radiatum and stratum oriens regions undergo significant atrophy, which is in agreement with earlier experimental findings (McEwen 1999; Vyas et al. 2002). Thus using this algorithm we are able transform a three-dimensional reconstruction of a real CA3 pyramidal neuron into one with varying percentages of atrophy, in a region-specific manner, relative to the original dendritic tree. This, in turn, provides a quantitative basis for comparing the passive and active membrane properties of model CA3 neurons with (i.e., Stress) and without (i.e., Control) region-specific dendritic atrophy.

Dendritic atrophy leads to increase in action potential firing rates

As a first step toward studying the impact of dendritic atrophy on active properties of CA3 neurons, we observe that the passive input resistance of the model CA3 pyramidal neuron, as measured from the soma, increases with dendritic atrophy (Fig. 1*B*). We find that the passive input resistance increases as an exponential function of the percentage of atrophy [$\tau = 11.08$, when fit with a function of the form $\exp(x/\tau)$]. As stress has been reported to elicit dissimilar patterns of atrophy along basal and apical dendrites (Watanabe et al. 1992), we also analyze the effects of inducing atrophy only in basal or apical dendrites (Fig. 1*B*). This analysis shows that, whereas both apical and basal atrophy lead to increase in input resistance, pruning the basal tree has a greater impact (exponential fit: apical: $\tau = 10.26 >$ basal: $\tau = 5.4$) in that it leads to a larger increase in input resistance for the same percentage of dendritic atrophy (Fig. 1*B*).

A direct consequence of greater input resistance of the cell would be an increase in its action potential firing rate. To test this prediction, we impose active properties on the model CA3 cell according to previously established criteria in the literature (described in METHODS). Thus this model CA3 neuron now combines both morphological and basic electrophysiological features that have been characterized using intracellular recordings in earlier studies (Hablitz and Johnston 1981; Migliore et al. 1995). Using this model under current-clamp conditions, we first replicate the two types of intrinsic patterns of action potential firing that have been observed experimentally in CA3 pyramidal neurons—regular spiking and bursting (Hablitz and Johnston 1981). An intrinsically bursting CA3 neuron responds to a brief pulse of somatic current injection with a series of action potentials placed close together in time, with reducing amplitudes, followed by a longer period of afterhyperpolarization. A regular spiking cell, on the other hand, responds with a single spike at regular intervals. These two cell types also repeat such bursting and regular-spiking behaviors with longer lasting current injections (Migliore et al. 1995). As has been reported in earlier electrophysiological and computational analyses (Migliore et al. 1995), an intrinsically spiking neuron differs from an intrinsically bursting neuron in terms of sodium and calcium-independent potassium channel conductances. These basic features, along with those mentioned in METHODS, are replicated in our model as well.

The intrinsically bursting CA3 neuron exhibits an increasing trend in rates of action potential firing evoked by somatic current injections of 0.15 nA (Fig. 1*C*). This increase in firing rates, mirroring what we observed earlier with passive resistance (Fig. 1*B*), is also more sensitive to atrophy in basal versus apical dendrites (Fig. 1*C*). The frequency of action potential firing approximately doubles within the range of stress-induced dendritic atrophy observed experimentally (3 Hz at 0% to 5.6 Hz at 35% atrophy).

We also find (data not shown) that similar atrophy-induced facilitation in firing rates is also observed in intrinsically bursting cells at a higher value of current injection (0.6 nA) when they switch to the regular-spiking mode. Finally, regular-spiking cells also display the same atrophy-induced increase in firing rates with somatic injections of low (0.15 nA) and high (0.6 nA) currents (data not shown). Hence, dendritic atrophy increases firing rates in a CA3 pyramidal neuron, irrespective of the levels of somatic current injections or its intrinsic firing modes.

[1] The online version of this article contains supplemental data.

Bursting CA3 neurons switch to regular spiking mode with progressive dendritic atrophy

Analyzing the effects of dendritic atrophy on the firing patterns of an intrinsically bursting CA3 pyramidal neuron, we observe that the neuron progressively switches to a regular spiking regime with greater dendritic atrophy (Fig. 1*D*). The quantitative features of this transition from bursting to spiking are depicted in Fig. 1*E*, where the average number of spikes per burst is plotted as a function of the percentage of dendritic atrophy. Representative traces for one such burst (Fig. 1*E, inset*), as a function of the percentage of dendritic atrophy, demonstrate that the number of spikes reduces from around four (typical for bursting mode) to one (regular spiking) with 45% atrophy (Fig. 1*E*).

How may this atrophy-induced switch from bursting to regular spiking pattern come about? In an effort to address this question we reasoned that stress-induced dendritic atrophy, through a reduction in dendritic surface area, leads to an overall decrease in the total numbers of channels (sum of the products of the density of a given channel in a given compartment and the compartment's surface area) that mediate the various currents underlying spiking patterns. Thus in principle, all of these conductances could contribute to the atrophy-induced transition from bursting to regular spiking patterns (as depicted in Fig. 1, *D* and *E*). Hence, to analyze the potential role of any specific ionic current in this switch, we varied each of them individually in the atrophied neuron to see what changes, if any, are able to restore the original bursting pattern seen in the unstressed control neuron. In other words, we examined if possible stress-induced plasticity in any of the individual ion channels was capable of preventing the switch from bursting to regular spiking behavior and in that process retaining firing rate and firing pattern homeostasis, despite the dendritic atrophy (35%). The results of this analysis, in which spikes were elicited through somatic injection of depolarizing currents, are summarized in Table 1. Two broad categories of changes in channel densities prevented this switch—one required an increase in N- or T-type calcium currents, whereas the other involved a decrease in the delayed rectifier potassium current (K_{DR}), the voltage- and calcium-dependent potassium channel (K_C) and the fast sodium current (Na). Noting that atrophy reduces the total values of individual currents, we reason that only those currents whose increase leads to firing pattern homeostasis are likely to counter the effects of atrophy. In other words, a reduction in the Ca_T and Ca_N currents, caused by an atrophy-induced loss in dendritic surface containing these calcium channels, provides a parsimonious explanation for the switch from bursting to regular spiking patterns (as depicted in Fig. 1*E*). Of course, this analysis does not rule out the possibility of other currents, either alone or in concert with others, contributing to homeostatic regulation of firing rates by undergoing modulations in channel properties or density. As Table 1 suggests, homeostasis in the rate and pattern of action potential firing can be controlled by different conductances to different degrees. Thus firing rate and bursting in these neurons are regulated by an intricate balance between multiple ion channel conductances (Migliore et al. 1995) and dendritic surface area (Fig. 1; Table 1). Therefore, within the context of stress, it should be noted that regulation of action potential firing rate and pattern could be regulated through ion channel plasticity, which may compensate for or exacerbate atrophy-induced changes in these measurements. Whereas Table 1 provides a broad parametric space for such possibilities, further experimental studies will be needed to examine the role of somato-dendritic ion channels in enabling or breaking such homeostasis at the single neuron level.

TABLE 1. *Modulation of individual current densities required for reversing the effects of 35% dendritic atrophy on action potential firing properties*

	Change in Channel Density Required to Maintain Control Values of	
Channel	Firing Rate	Average Number of Spikes per Burst
Na	22% decrease	50% decrease
K_{DR}	19% increase	32% decrease
K_A	25% increase	—
K_M	500% increase	—
Ca_T	—	160% increase
Ca_N	—	36% increase
Ca_L	—	—
K_{AHP}	67% increase	—
K_C	21% increase	63% decrease

Modulation of individual currents required for maintaining firing rate and firing pattern homeostasis in a neuron with 35% atrophy. Percentage and direction of changes (with respect to default control values) required in densities of various channels for an atrophied neuron to maintain "Control" levels of firing rate and average spikes per burst. This was analyzed by varying only one particular channel conductance at a time. —, indicates that changing only that conductance was not effective in reversing the atrophy-induced shifts in spiking properties. The L-type calcium channel does not affect either firing rate or the average number of spikes per burst because its perisomatic distribution (present only in compartments located ≤ 50 μm from the soma) is not affected by dendritic atrophy.

Effects of dendritic atrophy on synaptic potentials vary with stimulation and recordings sites

Next we investigate how synaptic inputs to CA3 pyramidal neurons may be influenced by dendritic remodeling. Specifically, we examine integration of excitatory postsynaptic potentials (EPSPs) along a passive dendritic tree. To this end, we add another dimension of biological detail at the synaptic level by performing simulations of AMPAR current injections at various locations on the dendritic tree (Fig. 2). We monitor the resultant EPSPs at the site of dendritic stimulation and at the soma (Fig. 2).

These simulations yield two distinct features of how processing of EPSPs by the atrophied CA3 neuron varies with dendritic location of the synaptic input. First, at the distal location (Fig. 2*B*), we do not detect a significant difference in the amplitude (V_{max}), rise-time (t^r), or decay-time (τ) of EPSPs. However, the impact of the same distal synaptic stimuli, when measured at the soma, is significantly greater in a neuron with 35% atrophy (Fig. 2*B*; increase in V_{max}: 38%). This indicates that, although the input impedance, as seen at the distal stimulation point, has not changed significantly, the amount of attenuation offered by the pathway from the distal dendritic stimulation point to the soma has been reduced by atrophy. Second, for more proximal inputs (Fig. 2*C*), a significant increase is observed in V_{max} at the somatic site (32% increase) and to a lesser extent at the dendritic recording sites as well (single EPSP: 12% increase). Furthermore, atrophy causes an

increase in the rise-time, t^r at both recording sites (somatic: 19% increase; dendritic: 6% increase) with proximal stimulation. Hence, for proximal synaptic stimulation, at distances where CA3 apical dendrites receive commissural/associational inputs, dendritic atrophy amplifies EPSPs at the site of the input and to a greater extent at the soma. In contrast, the amplifying effects of atrophy on more distal synaptic inputs are evident only at the soma. In summary, contrary to the commonly held notion that stress-induced dendritic atrophy may reduce synaptic inputs, it actually amplifies postsynaptic potentials.

Region-specific dendritic atrophy leads to region-specific increase in synaptic excitability

The above result raises the intriguing possibility of dendritic atrophy modulating the relative efficacy of distal and proximal stimulation in evoking synaptic responses. Does this imply that region-specific dendritic atrophy—the variations in atrophy based on dendritic location—may lead to modulation in synaptic excitability that is also region-specific? To probe this possibility in greater detail, we first divide up the dendritic tree into compartments of 50 μm segments according to their radial distance from the soma. Next, we measure somatic and local dendritic EPSPs evoked by a fixed AMPAR synaptic conductance (4 nS) along each of these dendritic compartments in control and atrophied passive trees. Finally, we group these EPSPs by the location of the dendritic segments from where they originated and carry out statistical comparisons between these EPSPs across dendritic trees with and without atrophy. Therefore, this analysis gives us detailed maps for comparing atrophied and control trees by way of variations in local dendritic (Fig. 2*D*) and somatic (Fig. 2*E*) EPSPs, as a function of the dendritic location of the AMPAR activation. This analysis shows that there is a significant increase in somatic EPSPs in response to AMPAR activation all along the atrophied tree compared with the control tree (Fig. 2*E*). By contrast, local dendritic EPSPs, especially those evoked by activation of distal locations, do not differ significantly (Fig. 2*D*). Although these data (Fig. 2, *D* and *E*) provide a continuous map of variations in EPSPs along the dendritic tree, the data depicted earlier in Fig. 2, *B* and *C,* reflect the same result, but by activating only two fixed dendritic locations (distal and proximal).

The results described above show that atrophied dendrites, when activated with the same synaptic AMPAR conductance, end up eliciting bigger somatic EPSPs compared with their control counterparts. This seems to suggest that atrophy causes a stronger coupling between the soma and the dendritic arbor emanating from it. To examine this possibility in greater detail, we adopted an approach that complements the one used earlier in Fig. 2, *D* and *E*. Instead of stimulating dendritic locations with a fixed synaptic conductance, we now set the somatic EPSP at a constant value and measure the minimum local dendritic voltage required to elicit this somatic EPSP of fixed size. Here too we use the same strategy of binning values in steps of 50 μm dendritic segments as in Fig. 2, *D* and *E*. This analysis shows a decrease in the minimum voltage necessary to evoke the same-sized somatic EPSP in a dendritic tree with an overall atrophy of 35% (Fig. 2*F*). Not surprisingly, although 35% atrophy causes the greatest reduction in this threshold, less severe atrophy in either the apical or basal dendrites alone do not have as big an effect on the threshold (Fig. 2*F*). Interestingly, the largest and statistically most significant differences between control and 35% atrophy are evident precisely in those dendritic segments that undergo the most pronounced atrophy—in the stratum radiatum region (100–350 μm from the soma, marked by dotted lines in Fig. 2*F*). To confirm that this is an effect of region-specific atrophy (Fig. 1; Supplementary Fig. S1), we perform the same simulations on trees subjected to apical-only and basal-only atrophy. Although apical-only atrophy leads to a large variation in the apical side and a smaller effect on the basal side, basal-only atrophy leads to the opposite effect (Fig. 2*F*), thus confirming that the region-specific increase in synaptic excitability is a direct effect of region-specific atrophy.

Taken together these results highlight two key features of the biophysical consequences of region-specific atrophy: *1*) the atrophied dendritic tree requires significantly smaller dendritic voltage (Fig. 2*F*), to elicit a somatic response of the same size as in the control neuron; and *2*) conversely, the same-sized synaptic conductance evokes a larger somatic response compared with that elicited in a control neuron (Fig. 2*E*). Both of these effects will contribute to a significant amplification in synaptic excitability after atrophy, the impact of which will be the most pronounced in dendritic segments undergoing greater atrophy.

Dendritic atrophy disrupts location independence of somatic EPSP amplitude

The above results raise an important question regarding the effects of dendritic filtering and the dependence of somatic EPSPs on the location of dendritic synapses. Direct dendritic recordings have shown that dendritic AMPAR conductance increases with distance from the soma, counterbalancing the effects of dendritic filtering and thereby normalizing somatic EPSP amplitude irrespective of dendritic location in a CA1 pyramidal cell (Hausser 2001; Magee and Cook 2000; Smith et al. 2003). Our results suggest that stress can disrupt this form of "dendritic democracy" that allows distal inputs to influence the somatic response to the same extent as more proximal inputs. Specifically, after chronic stress-induced atrophy, dendrites located in the stratum radiatum and beyond are capable of eliciting bigger somatic EPSPs (Fig. 2, *B* and *C*), thereby breaking down the equality between dendritic regions located at varying distances from the soma. As it has been shown that such normalization is brought about by a distance-dependent scaling of AMPAR conductance, we next analyze the minimum AMPAR conductance required at each dendritic point of a control and atrophied tree to elicit a somatic EPSP of the same amplitude, i.e., location independent somatic EPSPs. We find significant reductions in the minimal AMPA conductance required to elicit the same somatic EPSP in the atrophied tree (Fig. 2*G*). In other words, instead of atrophy making things worse for distal synaptic inputs, even smaller AMPAR conductances (compared with Control) are able to evoke the same somatic response after dendritic atrophy. Therefore, distally evoked synaptic inputs actually do better in terms of being heard at the soma after dendritic atrophy. We also observe a region-specific reduction in the minimum AMPAR conductance with atrophy, with larger reductions taking place farther away from the soma

in more distal dendritic segments (Fig. 2*G*). Region specificity of these reductions is also evident from simulations using trees with apical-only and basal-only atrophy (Fig. 2*G*). Thus atrophy localized to the stratum radiatum region of apical dendrites, for example, does not lead to extensive reductions (relative to Control) across the entire cell to the same degree. Instead, its greatest impact is manifested in the stratum radiatum and points more distal, with lesser effects on the basal side or closer to the soma. This is evident in the switch between the apical-only (Fig. 2*G*, green line) and basal-only (Fig. 2*G*, blue line) curves at the soma such that the values for the minimum AMPAR conductance with apical-only atrophy is higher on the basal side compared with those for basal-only atrophy and vice versa. This, in essence, is the region-specific nature of the synaptic hyperexcitability caused by region-specific atrophy of dendrites.

Finally, in keeping with previous experimental results (Smith et al. 2003), there is a reduction in the minimum AMPAR conductance with increasing distance from the soma (Fig. 2*G*). Thus our results suggest that dendritic atrophy disrupts the location independence of somatic EPSPs through an attenuation of dendritic filtering effects and consequent increase in the relative efficacy of distal inputs in exciting the soma. Taken together these results highlight two key features of the biophysical consequences of region-specific atrophy: *1*) the atrophied dendritic tree requires significantly smaller AMPAR conductance (Fig. 2*G*) and hence smaller dendritic voltage (Fig. 2*F*) to elicit a somatic response of the same size as in the control neuron; and *2*) conversely, the same-sized synaptic conductance evokes a larger somatic response compared with that elicited in a control neuron (Fig. 2*A*). Both of these effects will contribute to a significant amplification in synaptic excitability after atrophy, the impact of which will be the most pronounced in, but not necessarily confined to, dendritic segments undergoing the biggest atrophy. Although we have effectively used the notion of "dendritic democracy" and the underlying theoretical construct for showing the region-specificity of changes associated with region-specific dendritic atrophy, it should be noted that there is no experimental proof for the presence of such a gradient in AMPARs in the CA3 pyramidal neuron. Finally, although our analysis has focused on excitatory synapses for showing synaptic hyperexcitability and its region-specificity, such hyperexcitability would also affect inhibitory synapses in a similar manner.

Stress amplifies frequency-dependent summation of NMDA receptor–mediated EPSCs

The results above provide insights into the role of region-specific dendritic atrophy in modulating single EPSPs. As temporal summation is a crucial element in single neuron information processing, we next explored the role of stress in modulating temporal summation. As a first step, we used a similar methodology as in Fig. 2, *B* and *C*, whereby we choose representative control and atrophied neurons and analyze passive summation by injection multiple AMPA EPSCs at two distinct locations: one distal and other proximal location (Fig. 3*A*). We find our observations with single EPSC injection (Fig. 2, *B* and *C*) to be further confirmed with temporal summation as well (Fig. 3, *B* and *C*), with the effects being much larger than those observed with single EPSC injections. Specifically, the amount of temporal summation is higher in the atrophied tree than that in the Control dendritic tree. It may be also noted that the amount of attenuation offered by the pathway from the dendritic stimulation point (especially the distal stimulation point) to the soma is lesser in the atrophied tree (similar to the observations made with Fig. 2, *B* and *C*).

There is a large body of evidence showing that the frequency of stimulation, NMDA receptor (NMDAR) activation, and the temporal summation of resultant influx of calcium all play pivotal roles in determining the sign and magnitude of hippocampal synaptic plasticity mechanisms, such as LTP and LTD (Linden and Connor 1995; Lisman 2001; Malenka and Nicoll 1993). Various models of repeated stress impair hippocampal LTP (Kim and Diamond 2002). However, chronic stress also enhances the amplitude and decay time-constant of NMDAR-EPSCs at C/A synapses in area CA3 (Kole et al. 2002). Moreover, antidepressants that prevent stress-induced CA3 atrophy also reverse these specific changes in CA3 EPSCs, implying that stress-induced alterations in NMDAR signaling are likely to affect forms of hippocampal synaptic plasticity. Thus we analyze the specific effects of enhanced NMDAR-signaling in an atrophied CA3 neuron by using the same stimulation strategy described above (Fig. 3*B*). The total AMPAR conductance (spread across all compartments in the stratum radiatum) is set at a constant 10 nS, and the total NMDAR conductance is calculated according to the experimentally reported increase in the NMDA-EPSC/AMPA-EPSC ratio (Control: 0.26; Stress: 0.44), because AMPAR-EPSCs are not affected by stress (Kole et al. 2002). We also impose an increase in NMDA decay time-constant from 55 to 90 ms (Kole et al. 2002), along with 35% dendritic atrophy.

Figure 3*D* shows a typical example of AMPAR and NMDAR EPSCs obtained from Control and Stress cells using the above procedure. The small increase (Fig. 3*D*; ~14%; Control: −311 pA; Stress: −354 pA) observed in the AMPAR-EPSC in the Stress neuron is a reflection of the passive increase caused by 35% dendritic atrophy. The large increase (Fig. 3*D*; 105%; Control: 74 pA; Stress: 151 pA) observed in the NMDAR-EPSC, on the other hand, is the effect of all three parametric variations taken together. We also examined the effects of stress on temporal summation of NMDAR-EPSCs. Specifically, based on previously used experimental paradigms (Migliore et al. 1995; Philpot et al. 2001), we simulate the effects of applying 10 pulses at 100 Hz to activate synapses located in the stratum radiatum, of both Control and Stress cells. The direct effect of the enhanced amplitude and slower decay of the single NMDAR-EPSC (Fig. 4*A*) is clearly evident as an increase in the absolute amplitudes attained by the summated NMDAR-EPSCs in the Stress cell (Fig. 3*E*). In contrast, stress had no impact on temporal summation using a 1 Hz stimulation train (data not shown). Taken together, stress-induced changes in synaptic and intrinsic excitability appear to create favorable conditions for LTP-inducing stimuli rather than those leading to LTD. We will address the apparent conflict that this conclusion poses with respect to experimental observations on impaired stress-induced LTP in the DISCUSSION.

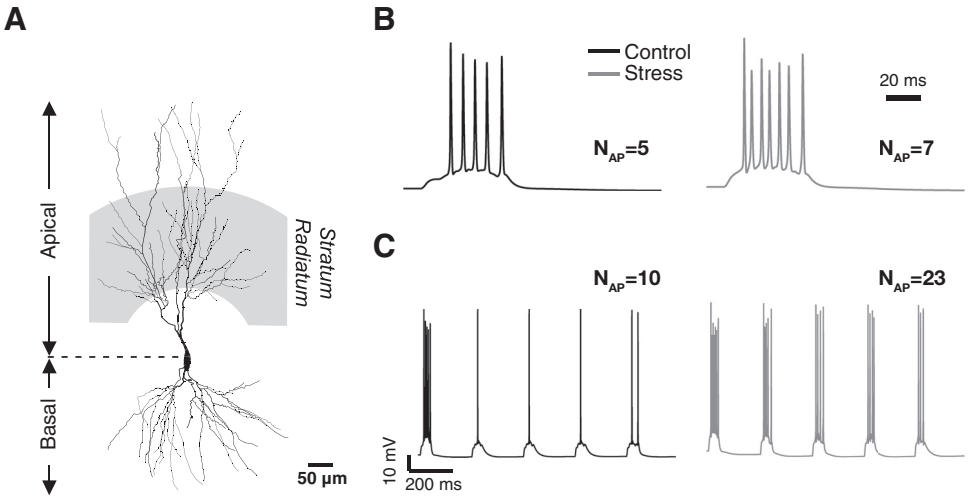

FIG. 4. Chronic immobilization stress amplifies single AMPAR and NMDAR EPSCs. *A*: representative neuron depicting the region of stimulation (shaded region; stratum radiatum) for eliciting synaptic responses in *B* and *C*. Somatic recordings (*top*, Control; *bottom*, Stress) of the spiking response elicited by 100 Hz synaptic stimulation lasting for 50 ms (*B*) and theta burst stimulation (*C*) of the stratum radiatum. Black, responses of "Control" neurons; Gray, responses from "Stress" neurons with 35% dendritic atrophy. In *B* and *C*, N_{AP} indicates the number of spikes observed in each case.

Dendritic atrophy increases number of spikes induced by synaptic stimulation

After evaluating the impact of atrophy on action potential firing and synaptic potentials, we integrate these two aspects by exploring the possibility that an increase in the amplitude of EPSPs in a passive dendritic tree could, in turn, enhance the probability of triggering somatic action potentials in a neuron with an active dendritic tree. To this end, we add another degree of biological detail to our model by imposing parameters for active conductances across the dendritic tree, again based on earlier experimental and computational studies (METHODS). Finally, we also incorporate the necessary details related to glutamatergic synaptic transmission on CA3 pyramidal neurons. Thus to these active dendritic arbors, we add synapses with co-localized NMDARs and AMPARs distributed over all dendritic compartments in stratum radiatum (Fig. 4*A*, shaded area). In the process of gradually building up our database on the range of effects elicited by dendritic atrophy, we have now arrived at a model CA3 pyramidal neuron that is endowed with several key morphological and physiological features established by earlier experimental reports. The final experimental detail we now add to our model is to change NMDAR EPSC properties, as in the experiments associated with Fig. 3. Therefore, taking all of these findings along with others mentioned earlier, a model stress-treated neuron, in this analysis, differs from a control in three important ways: *1*) 35% dendritic atrophy (Vyas et al. 2002); *2*) increase in the ratio of NMDAR- and AMPAR-EPSCs (NMDA/AMPA ratio) from 0.26 to 0.44 (Kole et al. 2002); and *3*) increase in NMDAR-EPSC decay time-constant, τ_{NMDA}, from 55 to 90 ms (Kole et al. 2002).

Next we apply synaptic stimulation (100 Hz train for 50 ms) to analyze the effects of atrophy on somatic voltage recordings. These simulations indicate that the above-mentioned synaptic changes, along with atrophy-induced changes in intrinsic excitability, enhance the number of spikes evoked by synaptic stimulation (Fig. 4*B*). As theta burst stimulation (TBS) is reported to be an optimal stimulation protocol for eliciting hippocampal LTP, we next explore the potential implications of these results for activity patterns that lead to hippocampal synaptic plasticity. To do this, we simulate the response of these CA3 neurons by applying theta burst stimulation (TBS: 5 pulses at 100 Hz, with burst frequency of 5 Hz) to the stratum radiatum, where stress-induced atrophy is known to be the most pronounced. The results using TBS also indicate that the probability of inducing an action potential, through synaptic activation, goes up with stress-induced atrophy (Fig. 3*C*). What may be the key factors contributing to this increase in the number of spikes? We find that dendritic atrophy alone is sufficient to elicit the increase in the number spikes and increases in either NMDA:AMPA ratio or NMDA-EPSC decay time-constant do not change the number of spikes (Supplemental Fig. S2). This is also consistent with our earlier result on atrophy-induced hyperexcitability presented in Fig. 1, *B* and *C*.

DISCUSSION

We have presented a model of stress-induced modulation of excitability in hippocampal CA3 pyramidal neurons that reconciles key experimental observations on the diverse morphological and physiological effects of chronic stress. In addition to explaining how stress-induced plasticity can lead to hyperexcitability, our findings provide a quantitative basis for translating a large body of morphological findings into the realm of specific electrophysiological measures of synaptic and intrinsic plasticity. Because most of the earlier electrophysiological studies examining the effects of stress have relied on extracellular field-potential recordings and have focused almost entirely on synaptic plasticity mechanisms such as LTP and LTD, our predictions regarding the impact of stress on nonsynaptic parameters related to intrinsic excitability point to new areas of investigation at the single-neuron level that have received little attention in the past.

Effects on intrinsic excitability

Despite a large body of experimental data on stress-induced dendritic atrophy, it has not been clear how such structural remodeling relates to hyperexcitability or excitotoxic damage (Conrad et al. 2004), another key factor that has been presumed to underlie hippocampal dysfunction following chronic stress (McEwen 1999). Our computational analysis on how stress-induced atrophy of CA3 dendrites can lead to an increase in the intrinsic excitability of these neurons give rise to two broad classes of findings: some that are consistent with previous

experimental data and others that provide specific predictions. The following experimental reports are in agreement with some of the predictions emerging from our results:

1) A study that used whole cell recordings from CA3 pyramidal neurons showed that repeated restraint stress leads to ~20% increase in input resistance and ~30% apical dendritic atrophy (Kole et al. 2004), which is broadly consistent with our prediction (Fig. 1).

2) Another study, reporting an increase in the percentage of nonbursting CA3 cells with chronic treatment of corticosteroids (Okuhara and Beck 1998), lends indirect experimental support for our prediction that bursting cells switch over to a regular spiking regime with stress (Fig. 1*D*).

3) Our analysis here has also identified dendritic atrophy, and not NMDAR-related parameters, as the key factor behind the increase in spiking elicited by synaptic activation (Fig. 4; Supplemental Fig. S2). Based on these observations on the increase in burst durations and the number of spikes fired (Fig. 4; Supplemental Fig. S2), we postulate that the vulnerability of the CA3 network to hyperexcitability should be considerably enhanced with stress. Consistent with this, it has been reported that high-frequency stimulation of the commissural/associational inputs to CA3 causes epileptic afterdischarges in a greater percentage of stressed rats relative to nonstressed control rats (Pavlides et al. 2002).

4) A recent study also shows that chronic stress exacerbates ibotenic acid–induced lesions selectively within the CA3 region (Conrad et al. 2004). This is consistent with our prediction that the CA3 neurons, and hence the auto-associative network formed by them are hyperexcitable after stress.

Hyperexcitability, saturation of LTP, and metaplasticity

Results presented here suggest that chronic stress facilitates conditions that clearly tilt the balance of plasticity toward eliciting greater LTP across a range of stimulus frequencies without affecting LTD-inducing stimuli (e.g., 1 Hz). Why then has a majority of experimental studies reported stress-induced impairment of LTP? The most plausible explanation comes from the theoretical framework offered by the Bienenstock-Cooper-Munro (BCM) rule for synaptic plasticity (Bienenstock et al. 1982). According to this rule, the threshold for induction of LTP is itself modifiable and is directly related to the average postsynaptic activity (Abraham and Bear 1996; Bienenstock et al. 1982). Our findings suggest two mechanisms through which chronic stress could alter this threshold. First, the saturation of LTP along with increased synaptic excitability would lead to an increase in postsynaptic activity, a direct correlate of increased synaptic strengths. Second, the increase in intrinsic excitability of individual neurons, through enhanced CA3 recurrent network activity, could contribute to greater postsynaptic activity. This cumulative increase in postsynaptic activity, under the BCM framework, would shift the plasticity profile to the right, thereby raising the threshold for subsequent LTP induction. This, in turn, would be manifested as a reduction or inhibition of subsequent LTP and also favor depression of synaptic strength through LTD (Kim and Yoon 1998), thereby mediating hyperexcitability-induced metaplasticity at these synapses. While such a scenario based on the BCM theory has been proposed earlier (Diamond et al. 2004; Kim and Yoon 1998) in the context of stress-induced metaplasticity, our results provide a rigorous biophysical basis for explaining how such a metaplastic shift can be caused by specific stress-induced changes in CA3 neuronal structure and physiology.

Although previous studies have characterized the inhibition of hippocampal LTP caused by various stressors, a systematic investigation of chronic stress-induced metaplasticity (Kim and Yoon 1998) has not been carried out. Moreover, a majority of reports on stress-induced impairment of LTP are not from area CA3, which undergoes the most significant atrophy among all hippocampal regions. However, results that are strongly suggestive of the scenario presented above come from in vitro and in vivo studies in area CA1 showing impaired LTP, but enhanced LTD, following various forms of acute stress (Kim et al. 1996). Hence, if a rigorous experimental analysis of LTP/D at commissural/associational-CA3 synapses is carried out, our results predict that chronic stress would lead to a rightward shift in the modification threshold of the BCM-like plasticity profile.

Experimentally observed increases in the duration and amplitude of NMDAR-mediated currents (Kole et al. 2002) could lead to a loss of specificity due to a broadening in width of the time-window for coincidence detection. Furthermore, based on our results on region-specific differences in the spread of synaptic properties, combined with the reported location dependence of spike-timing dependent plasticity (STDP) (Froemke et al. 2005), we predict that stress-induced differences in STDP could also display region-specificity, i.e., not all dendritic segments will be affected equally in terms of their ability to sustain optimal STDP after stress.

Although the BCM rule has served as a very useful formalism for studying metaplasticity of synapses, recent experimental evidence has opened up the possibility that changes in dendritic excitability can also act as a substrate for metaplasticity (Abraham 2008; Frick and Johnston 2005; Johnston and Narayanan 2008; Kim and Linden 2007). In this context, our results on the modulation of synaptic excitability by dendritic remodeling highlight the need to probe the effects of structural plasticity on metaplasticity, a question that is yet to be explored in detail. Moreover, based on the current study, we predict that such metaplastic changes could be selective and be dependent on the specific dendritic region where such remodeling occurs. Such localized changes have significant computational implications for the storage capacity and encoding capabilities of a single neuron, especially given that plasticity in intrinsic properties is now widely acknowledged as a putative cellular correlate for learning and memory (Abraham 2008; Frick and Johnston 2005; Frick et al. 2004; Johnston and Narayanan 2008; Kim and Linden 2007; Poirazi and Mel 2001; Sjostrom et al. 2008; Zhang and Linden 2003).

Functional implications for stress-induced memory deficits

Functionally, information processing within a single CA3 pyramidal neuron is dependent on spatiotemporal summation of mossy fiber inputs from the dentate gyrus, perforant path inputs from the entorhinal cortex, the commissural/associational inputs from the CA3, and inhibitory connections from multiple interneurons (Johnston and Amaral 2004). The relative efficacy of inputs from each of these different regions is driven by multiple factors, with dendritic arborization playing a major role (Mainen and Sejnowski 1996; Sjostrom et al.

2008), especially given the segregation of these inputs into different strata (Johnston and Amaral 2004). Our results suggest that region-specific changes to dendritic arborization lead to region-specific changes in synaptic efficacy as well (Fig. 2*F*). Such region-specific changes have implications to the interactions between entorhinal inputs to the stratum lacunosum moleculare and the commissural/associational inputs to the stratum radiatum of a CA3 pyramidal neuron. Specifically, such plasticity would alter the relative efficacy of perforant path inputs with respect to their commissural/associational counterparts, which, in turn, would affect learning tasks mediated by the hippocampal formation (Nakashiba et al. 2008).

Growing evidence from various knockout mouse models has identified a critical role for NMDA receptors at CA3 commissural/associational inputs in specific forms of hippocampal-dependent learning and memory (Nakashiba et al. 2008; Nakazawa et al. 2002). Furthermore, in vivo tetrode recordings of place cell activity also indicate that disruption of NMDAR-dependent LTP/LTD can modulate various properties of hippocampal receptive fields including their size, specificity, and structure (Mehta et al. 2000; Nakazawa et al. 2002). Accumulating theoretical and experimental evidence has also given rise to models of hippocampal function that emphasize a critical role for bidirectional modifiability of synaptic strength in supporting an effective memory system (Bliss and Collingridge 1993; Migaud et al. 1998; Neves et al. 2008; Willshaw and Dayan 1990; Zeng et al. 2001). However, more recent studies also point to the important role of intrinsic properties in modulating synaptic efficacy and plasticity in neurons (Abraham 2008; Frick and Johnston 2005; Johnston and Narayanan 2008; Kim and Linden 2007; Sjostrom et al. 2008; Zhang and Linden 2003). In light of results presented here, these alternate mechanisms could provide valuable insights on how synaptic and intrinsic properties work together in establishing behaviorally relevant computations within individual neurons and their networks and how these may lead to the deleterious effects observed in pathological conditions like chronic stress (Beck and Yaari 2008).

Testable predictions and future directions

The analyses presented here provide a number of predictions that can be tested experimentally. First, the question of atrophy-induced increase in excitability and switch in firing patterns (Fig. 1) could be directly tested using electrophysiological recordings from CA3 pyramidal neurons in control and stressed animals (Kole et al. 2004). The results from such experiments would help understand the relative balance between atrophy and possible changes in voltage-gated ion channel properties in regulating neuronal excitability and firing patterns in animals exposed to chronic stress (Table 1). Next, direct dual dendritic recordings in CA3 pyramidal neurons from control and stressed animals could be used to ask if region-specific dendritic atrophy leads to region-specific hyperexcitability (Figs. 2 and 3). Such analysis coupled with synaptic stimulation (Magee and Cook 2000; Smith et al. 2003) would also test whether alterations in "dendritic democracy" and associated redistribution of AMPAR conductance are affected by region-specific dendritic atrophy (Fig. 2*G*). Finally, a systematic analysis of the profile of synaptic plasticity as a function of stimulus frequency (Dudek and Bear 1992; Johnston et al. 2003) in CA3 neurons could be used to test whether there is indeed a stress-induced shift in the LTP/D threshold within the broader context of a BCM-like framework. Similar experiments involving saturation of LTP could be employed to explore the possibility that LTP saturation is altered as a result of atrophy-induced hyperexcitability.

Although our study aims at providing a quantitative basis for linking morphological and receptor/channel-level changes to aberrations in synaptic plasticity, it does not take into account all the possible variables that are likely to be affected by stress. Some of the simplifying assumptions made in this model also point to a lack of quantitative experimental data on several key parameters and need rigorous experimental studies for better understanding of the cellular effects of chronic stress. For instance, little is known about the impact of stress on gene expression patterns that are also likely to modulate structural and physiological markers of stress-induced plasticity. Furthermore, although much of the experimental evidence on stress-induced morphological plasticity has focused on dendritic remodeling, nothing is known about how stress affects axonal arbors and connectivity patterns. Therefore, in addition to stress-induced modulation of postsynaptic excitability analyzed in our study, presynaptic changes could also play an important role and require further analysis. Finally, although our results suggest that dendritic atrophy and its modulation of intrinsic excitability can have an impact on the threshold for LTP/D induction, other stress-induced changes in biochemical signaling pathways underlying LTP/D could also contribute to such mechanisms. These biochemical signaling mechanisms, apart from playing a role in altering synaptic plasticity, could also mediate trafficking and plasticity of voltage-gated ion channels, thereby affecting intrinsic excitability and synaptic plasticity (Johnston and Narayanan 2008; Kim and Linden 2007; Vacher et al. 2008).

In conclusion, the prevailing framework for examining the functional consequences of stress-induced dendritic atrophy has been driven by the logic that a reduction in postsynaptic dendritic surface will adversely affect the availability of synaptic inputs and thereby synaptic plasticity. This approach has focused primarily on stress-induced changes in synaptic weights, thereby overlooking the impact of region-specific structural plasticity of dendrites on intrinsic excitability of neurons. Moreover, these two measures of stress-induced plasticity have often been treated as separate parameters contributing independently to hippocampal dysfunction. Our results show that these two key measures of stress-induced hippocampal plasticity converge and interact in ways that can profoundly alter important forms of intrinsic and synaptic plasticity in the hippocampus. These changes, through direct modulation of intrinsic and synaptic excitability and through indirect changes in metaplastic shifts, could act as putative substrates for stress-induced deficits in behavioral function (Abraham 2008; Johnston and Narayanan 2008; Kim and Yoon 1998; Kim and Linden 2007; McEwen 1999; Sjostrom et al. 2008; Zhang and Linden 2003). Therefore, our findings support a model where stress-induced amplification of intrinsic and synaptic excitability may impair hippocampal learning and memory by directly altering integration of information within a single neuron and by indirectly disrupting the balance of bidirectional synaptic plasticity.

ACKNOWLEDGMENTS

Present address of R. Narayanan: Molecular Biophysics Unit, Indian Institute of Science, Bangalore 560012, India.

GRANTS

R. Narayanan was supported by a research fellowship from the Department of Biotechnology, India, and S. Chattarji was supported by an International Senior Research Fellowship from the Wellcome Trust, United Kingdom.

DISCLOSURES

No conflicts of interest are declared by the authors.

REFERENCES

Abraham WC. Metaplasticity: tuning synapses and networks for plasticity. *Nat Rev Neurosci* 9: 387, 2008.

Abraham WC, Bear MF. Metaplasticity: the plasticity of synaptic plasticity. *Trends Neurosci* 19: 126–130, 1996.

Beck H, Yaari Y. Plasticity of intrinsic neuronal properties in CNS disorders. *Nat Rev Neurosci* 9: 357–369, 2008.

Bienenstock EL, Cooper LN, Munro PW. Theory for the development of neuron selectivity: orientation specificity and binocular interaction in visual cortex. *J Neurosci* 2: 32–48, 1982.

Bliss TV, Collingridge GL. A synaptic model of memory: long-term potentiation in the hippocampus. *Nature* 361: 31–39, 1993.

Cannon RC, Turner DA, Pyapali GK, Wheal HV. An on-line archive of reconstructed hippocampal neurons. *J Neurosci Methods* 84: 49–54, 1998.

Collingridge GL, Kehl SJ, McLennan H. Excitatory amino acids in synaptic transmission in the Schaffer collateral-commissural pathway of the rat hippocampus. *J Physiol* 334: 33–46, 1983.

Conrad CD, Jackson JL, Wise LS. Chronic stress enhances ibotenic acid-induced damage selectively within the hippocampal CA3 region of male, but not female rats. *Neuroscience* 125: 759–767, 2004.

Debanne D, Gahwiler BH, Thompson SM. Long-term synaptic plasticity between pairs of individual CA3 pyramidal cells in rat hippocampal slice cultures. *J Physiol* 507: 237–247, 1998.

Destexhe A, Mainen ZF, Sejnowski TJ. Kinetic models of synaptic transmission. In: *Methods in Neuronal Modeling: From Ions to Network*, edited by Koch C, Segev I. Cambridge, MA: MIT Press, 1998, p. 1–25.

Diamond DM, Park CR, Woodson JC. Stress generates emotional memories and retrograde amnesia by inducing an endogenous form of hippocampal LTP. *Hippocampus* 14: 281–291, 2004.

Dudek SM, Bear MF. Homosynaptic long-term depression in area CA1 of hippocampus and effects of N-methyl-D-aspartate receptor blockade. *Proc Natl Acad Sci USA* 89: 4363–4367, 1992.

Frick A, Johnston D. Plasticity of dendritic excitability. *J Neurobiol* 64: 100–115, 2005.

Frick A, Magee J, Johnston D. LTP is accompanied by an enhanced local excitability of pyramidal neuron dendrites. *Nat Neurosci* 7: 126–135, 2004.

Froemke RC, Poo MM, Dan Y. Spike-timing-dependent synaptic plasticity depends on dendritic location. *Nature* 434: 221–225, 2005.

Hablitz JJ, Johnston D. Endogenous nature of spontaneous bursting in hippocampal pyramidal neurons. *Cell Mol Neurobiol* 1: 325–334, 1981.

Hausser M. Synaptic function: dendritic democracy. *Curr Biol* 11: R10–R12, 2001.

Hines ML, Carnevale NT. The NEURON simulation environment. *Neural Comput* 9: 1179–1209, 1997.

Hines ML, Carnevale NT. Expanding NEURON's repertoire of mechanisms with NMODL. *Neural Comput* 12: 995–1007, 2000.

Jahr CE, Stevens CF. Voltage dependence of NMDA-activated macroscopic conductances predicted by single-channel kinetics. *J Neurosci* 10: 3178–3182, 1990.

Johnston D, Amaral DG. Hippocampus. In: *Synaptic Organization of the Brain*, edited by Shepherd G. New York: Oxford, 2004, p. 455–498.

Johnston D, Christie BR, Frick A, Gray R, Hoffman DA, Schexnayder LK, Watanabe S, Yuan LL. Active dendrites, potassium channels and synaptic plasticity. *Philos Trans R Soc Lond B Biol Sci* 358: 667–674, 2003.

Johnston D, Narayanan R. Active dendrites: colorful wings of the mysterious butterflies. *Trends Neurosci* 31: 309–316, 2008.

Kim JJ, Diamond DM. The stressed hippocampus, synaptic plasticity and lost memories. *Nat Rev Neurosci* 3: 453–462, 2002.

Kim JJ, Foy MR, Thompson RF. Behavioral stress modifies hippocampal plasticity through N-methyl-D-aspartate receptor activation. *Proc Natl Acad Sci USA* 93: 4750–4753, 1996.

Kim JJ, Yoon KS. Stress: metaplastic effects in the hippocampus. *Trends Neurosci* 21: 505–509, 1998.

Kim SJ, Linden DJ. Ubiquitous plasticity and memory storage. *Neuron* 56: 582–592, 2007.

Kole MH, Costoli T, Koolhaas JM, Fuchs E. Bidirectional shift in the cornu ammonis 3 pyramidal dendritic organization following brief stress. *Neuroscience* 125: 337–347, 2004.

Kole MH, Swan L, Fuchs E. The antidepressant tianeptine persistently modulates glutamate receptor currents of the hippocampal CA3 commissural associational synapse in chronically stressed rats. *Eur J Neurosci* 16: 807–816, 2002.

Krichmar JL, Nasuto SJ, Scorcioni R, Washington SD, Ascoli GA. Effects of dendritic morphology on CA3 pyramidal cell electrophysiology: a simulation study. *Brain Res* 941: 11–28, 2002.

Linden DJ, Connor JA. Long-term synaptic depression. *Annu Rev Neurosci* 18: 319–357, 1995.

Lisman JE. Three Ca^{2+} levels affect plasticity differently: the LTP zone, the LTD zone and no man's land. *J Physiol* 532: 285, 2001.

Magarinos AM, McEwen BS. Stress-induced atrophy of apical dendrites of hippocampal CA3c neurons: comparison of stressors. *Neuroscience* 69: 83–88, 1995a.

Magarinos AM, McEwen BS. Stress-induced atrophy of apical dendrites of hippocampal CA3c neurons: involvement of glucocorticoid secretion and excitatory amino acid receptors. *Neuroscience* 69: 89–98, 1995b.

Magarinos AM, McEwen BS, Flugge G, Fuchs E. Chronic psychosocial stress causes apical dendritic atrophy of hippocampal CA3 pyramidal neurons in subordinate tree shrews. *J Neurosci* 16: 3534–3540, 1996.

Magee JC, Cook EP. Somatic EPSP amplitude is independent of synapse location in hippocampal pyramidal neurons. *Nat Neurosci* 3: 895–903, 2000.

Magee JC, Johnston D. Characterization of single voltage-gated Na^+ and Ca^{2+} channels in apical dendrites of rat CA1 pyramidal neurons. *J Physiol* 487: 67–90, 1995.

Mainen ZF, Sejnowski TJ. Influence of dendritic structure on firing pattern in model neocortical neurons. *Nature* 382: 363–366, 1996.

Malenka RC, Nicoll RA. NMDA-receptor-dependent synaptic plasticity: multiple forms and mechanisms. *Trends Neurosci* 16: 521–527, 1993.

McEwen BS. Stress and hippocampal plasticity. *Annu Rev Neurosci* 22: 105–122, 1999.

Mehta MR, Quirk MC, Wilson MA. Experience-dependent asymmetric shape of hippocampal receptive fields. *Neuron* 25: 707–715, 2000.

Migaud M, Charlesworth P, Dempster M, Webster LC, Watabe AM, Makhinson M, He Y, Ramsay MF, Morris RG, Morrison JH, O'Dell TJ, Grant SG. Enhanced long-term potentiation and impaired learning in mice with mutant postsynaptic density-95 protein. *Nature* 396: 433–439, 1998.

Migliore M, Cook EP, Jaffe DB, Turner DA, Johnston D. Computer simulations of morphologically reconstructed CA3 hippocampal neurons. *J Neurophysiol* 73: 1157–1168, 1995.

Migliore M, Hoffman DA, Magee JC, Johnston D. Role of an A-type K^+ conductance in the back-propagation of action potentials in the dendrites of hippocampal pyramidal neurons. *J Comput Neurosci* 7: 5–15, 1999.

Nakashiba T, Young JZ, McHugh TJ, Buhl DL, Tonegawa S. Transgenic inhibition of synaptic transmission reveals role of CA3 output in hippocampal learning. *Science* 319: 1260–1264, 2008.

Nakazawa K, Quirk MC, Chitwood RA, Watanabe M, Yeckel MF, Sun LD, Kato A, Carr CA, Johnston D, Wilson MA, Tonegawa S. Requirement for hippocampal CA3 NMDA receptors in associative memory recall. *Science* 297: 211–218, 2002.

Narayanan R, Narayan A, Chattarji S. A probabilistic framework for region-specific remodeling of dendrites in three-dimensional neuronal reconstructions. *Neural Comput* 17: 75–96, 2005.

Neves G, Cooke SF, Bliss TV. Synaptic plasticity, memory and the hippocampus: a neural network approach to causality. *Nat Rev Neurosci* 9: 65–75, 2008.

Okuhara DY, Beck SG. Corticosteroids influence the action potential firing pattern of hippocampal subfield CA3 pyramidal cells. *Neuroendocrinology* 67: 58–66, 1998.

Pavlides C, Nivon LG, McEwen BS. Effects of chronic stress on hippocampal long-term potentiation. *Hippocampus* 12: 245–257, 2002.

Philpot BD, Sekhar AK, Shouval HZ, Bear MF. Visual experience and deprivation bidirectionally modify the composition and function of NMDA receptors in visual cortex. *Neuron* 29: 157–169, 2001.

Poirazi P, Mel BW. Impact of active dendrites and structural plasticity on the memory capacity of neural tissue. *Neuron* 29: 779–796, 2001.

Sapolsky RM. Depression, antidepressants, and the shrinking hippocampus. *Proc Natl Acad Sci USA* 98: 12320–12322, 2001.

Sapolsky RM. Chickens, eggs and hippocampal atrophy. *Nat Neurosci* 5: 1111–1113, 2002.

Sjostrom PJ, Rancz EA, Roth A, Hausser M. Dendritic excitability and synaptic plasticity. *Physiol Rev* 88: 769–840, 2008.

Smith MA, Ellis-Davies GC, Magee JC. Mechanism of the distance-dependent scaling of Schaffer collateral synapses in rat CA1 pyramidal neurons. *J Physiol* 548: 245–258, 2003.

Traub RD, Borck C, Colling SB, Jefferys JG. On the structure of ictal events in vitro. *Epilepsia* 37: 879–891, 1996.

Vacher H, Mohapatra DP, Trimmer JS. Localization and targeting of voltage-dependent ion channels in mammalian central neurons. *Physiol Rev* 88: 1407–1447, 2008.

van Ooyen A, Duijnhouwer J, Remme MW, van Pelt J. The effect of dendritic topology on firing patterns in model neurons. *Network* 13: 311–325, 2002.

Vetter P, Roth A, Hausser M. Propagation of action potentials in dendrites depends on dendritic morphology. *J Neurophysiol* 85: 926–937, 2001.

Vyas A, Mitra R, Shankaranarayana Rao BS, Chattarji S. Chronic stress induces contrasting patterns of dendritic remodeling in hippocampal and amygdaloid neurons. *J Neurosci* 22: 6810–6818, 2002.

Watanabe Y, Gould E, McEwen BS. Stress induces atrophy of apical dendrites of hippocampal CA3 pyramidal neurons. *Brain Res* 588: 341–345, 1992.

Willshaw DJ, Dayan P. Optimal plasticity in matrix memories: what goes up must come down. *Neural Comput* 2: 85–93, 1990.

Wong RK, Prince DA. Participation of calcium spikes during intrinsic burst firing in hippocampal neurons. *Brain Res* 159: 385–390, 1978.

Zeng H, Chattarji S, Barbarosie M, Rondi-Reig L, Philpot BD, Miyakawa T, Bear MF, Tonegawa S. Forebrain-specific calcineurin knockout selectively impairs bidirectional synaptic plasticity and working/episodic-like memory. *Cell* 107: 617–629, 2001.

Zhang W, Linden DJ. The other side of the engram: experience-driven changes in neuronal intrinsic excitability. *Nat Rev Neurosci* 4: 885–900, 2003.